International Journal of Concrete Structures and Materials

RESEARCH

Open Access

Experimental and Numerical Investigations of Punching Shear Strengthening of Slab-Circular Column Connection Incorporating UHPC and Galvanized Threaded Steel Bolts

Ahmed Hamoda[1*], Khaled Sennah[2], Mizan Ahmed[3], Aref A. Abadel[4] and Mohamed Emara[5,6]

Abstract

Punching shear failure poses a critical risk in flat slab–column structures, potentially leading to catastrophic collapses. Retrofitting methods typically involve flexural or shear strengthening. Recent studies, however, reveal that combining indirect flexural strengthening with direct shear strengthening augments the punching shear performance. This research employed ultra-high-performance engineered cementitious composites (UHP-ECC) and ultra-high-performance steel-fiber-reinforced concrete (UHP-SFRC) as a bonded layer on the slab's compression zone confining column as indirect flexural strengthening and galvanized threaded steel bolts as direct shear strengthening through slab thickness to augment the punching shear capacity. Six square flat slabs with central circular columns were constructed and then experimented to collapse to verify the effect of this proposed strengthening technique. The effects of various mesh and concrete types are investigated. Results showed that combining the UHP-ECC or UHP-SFRC bonded layer in the compression side with bonded galvanized threaded steel bolts significantly enhanced the punching shear strength of the slabs. The experimental findings demonstrated a remarkable increase of 62% and 111% over the unstrengthened slab for the UHP-ECC and UHP-SFRC strengthened slabs with single-layer mesh, respectively. Further enhancements were observed by adding a second steel reinforcement mesh to the UHP-bonded layer. A numerical model was developed using the finite-element (FEM) method to predict the structural behavior of tested slabs. Numerical results revealed that the FEM predicts well the performance of the slab–column connection, aligning well with experimental findings.

Keywords Flat slab, Flexural strengthening, Shear strengthening, Punching shear, Ultra-high-performance, Engineered cementitious composites

Journal information: ISSN 1976-0485 / eISSN 2234-1315.

*Correspondence:
Ahmed Hamoda
ahmed_hamoda@eng.kfs.edu.eg
Full list of author information is available at the end of the article

1 Introduction

Punching shear in reinforced concrete (RC) flat slabs is a crucial structural engineering concern, especially in high-rise buildings, because it can cause unexpected catastrophic failures (Jang & Kang, 2019; Song et al., 2012). Numerous researchers dealt with strengthening flat slab structures to augment the punching shear capacity using traditional and innovative techniques. A few authors summarized the available strengthening techniques for RC flat slab structures resisting punching shear collapse (Lapi et al., 2018; Saleh et al., 2018a; Yagar et al., 2024). These strengthening techniques include (i) direct punching shear upgrading by enhancing shear strength through implemented shear reinforcements through the slab depth, (ii) indirect punching shear strengthening by improving flexural strength through increasing slab flexural reinforcement, (iii) combined shear and flexural strengthening, and (iv) enlargement of the supporting columns. The enlargement of the supporting column can be achieved by post-installing a steel capital, casting a concrete column head, or widening the column. Muttoni (2008) showed that doubling the existing supporting column size increases the punching shear capacity by 30% to 50% due to increasing the critical perimeter of the punching shear failure plane after strengthening. This approach is not affected by the quantity of flexural reinforcement present in the slab, unlike other strengthening techniques (Muttoni, 2008).

Post-installed bolts can be used as a direct punching shear strengthening method. This can be achieved by drilling holes through the slab depth around the column, then putting the bolts through the holes and securing them to the top and bottom concrete soffits using steel nuts. Few authors investigated experimentally the retrofitting of flat slab structures suffering punching shear employing post-installed steel dowels (Bolešová & Gajdošová, 2023; El-Sayed et al., 2016; Fernández Ruiz et al., 2010; Said et al., 2020; Saleh et al., 2018b; Taresh et al., 2021). Fiber-reinforced polymers (FRP) for retrofitting slab–column connections have recently observed significant attention as direct FRP strengthening techniques to overcome punching shear failure in flat slab structures around columns. This technique involves drilling holes through the slab thickness and inserting bonded FRP reinforcement. This methodology incorporates the post-installation of FRP studs, FRP dowels, FRP strips, FRP fans, FRP grid, and FRP external stirrups as shear reinforcement (da Silva Rodrigues et al., 2015; El-Kashif et al., 2019; Erdogan et al., 2010; Jafarian et al., 2020; Koppitz et al., 2014; Lawler & Polak, 2011; Li et al., 2007; Meisami et al., 2013, 2014, 2015; Said et al., 2020; Santos et al., 2019; Smith et al., 2011; Zhang & Smith, 2012). Flexural strengthening of flat slab structures around columns includes near-surface mounted reinforcement (NSMR) (Abdel-Kareem, 2020), externally bonded reinforcement on Grooves (Amiri & Talaeitaba, 2020; Azizi & Talaeitaba, 2019), and externally bonded FRP strips (Abdulrahman et al., 2017; Al-Mawed & Hamad, 2023; Chen & Chen, 2019; Dat & Hieu, 2023; Durucan & Anil, 2015; El-Enein et al., 2014; Halabi et al., 2013; Polies et al., 2010; Qian & Li, 2013). Research showed that premature debonding failure may occur in the case of externally bonded FRP strip strengthening. Anchorage regimes like anchoring studs beside FRP end anchors eliminate debonding together with improve the flexural amplitude of the slab–column connection (Akhundzada et al., 2019; Silva et al., 2019, 2021). Abdullah et al. (Abdullah & Bailey, 2018; Abdullah et al., 2013) investigated the punching shear resistance of a column-slab region strengthened with prestressed or non-prestressed FRP strips. They concluded that external prestressed FRP strengthening often causes debonding due to attaining the FRP strips' higher strain level. Lapi et al. (2019) investigated scenarios that were mostly delivered to enhance punching shear failure. It was concluded that flexural strengthening using FRP contributes to increasing the punching shear resistance. The post-strengthening load–rotation curve exhibits increased stiffness due to the augmented flexural reinforcement. Strengthening the flat slab in flexure indirectly improves its punching shear resistance by improving the strengthened slab's post-cracking stiffness. In another study, Harajli and Soudki (2003) showed that the punching shear capacity increased by 45% compared to the control slab when using orthogonally arranged carbon fiber-reinforced polymer (CFRP) strips in each direction.

The ACI 318–19 (2019) specifies equations for the punching shear strength of slab-beam connection that ignore the effect of flexural reinforcement. Conservatively, one may calculate the punching shear capacity of flat slabs augmented with FRP strips bonded externally according to both ACI 318–19 (2019) and ACI 440.2R-17 (2017) by neglecting the contribution of the FRP strips in augmenting the punching shear capacity. It was reported the significant contribution of FRP in flexural strengthening on punching performance by researchers previously (Chen & Li, 2005; Farghaly & Ueda, 2011; Faria et al., 2014). Some researchers came up with modifications to include the FRP flexural strengthening effect on the punching shear capacity in the form of effective reinforcement ratio and equivalent effective depth. Abdulrahman and Aziz (2021), and Yagar et al. (2024) evaluated the accuracy of the ACI 318–19 code equation for punching shear performance with the modified versions made by Chen and Li (2005), Farghaly and Ueda (2011), and Faria et al. (2014) using experimental test

results. They also developed a new formula for predicting the punching shear capacity of flat slab–column connections in the absence of accurate design models. Hamoda et al. (2024d) conducted an experimental and numerical examination to enhance the punching shear performance by strengthening the tension side surface with CFRP strips and ultra-high performance ECC. The results indicated that the bonded CFRP strips influenced the load–deformation response without significantly altering the failure criterion caused by punching shear.

In direct shear strengthening, shear anchors/bolts would push the punching shear failure plane further away from the perimeter of the column due to the increased punching shear capacity provided by the shear reinforcement. Consequently, external flexural strengthening can be combined with additional vertical shear reinforcement to increase the deformation and shear capacities to a greater value. Binici and Bayrak (2003), and Sissakis and Sheikh (2007) used external CFRP stirrups combined with CFRP sheets bonded to the slab tension side to enhance the punching shear capacity of the slab–column region. El-Salakawy et al. (2004), and Harajli et al. (2006) investigated experimentally strengthening interior slab–column connections using a combination of FRP sheets bonded to the tension side of the slab and steel bolts through the slab thickness. Torabian et al. (2020, 2021) investigated experimentally the performance of slab–column connection that was strengthened with post-installed bolts combined with externally bonded reinforcement in grooves using CFRP sheets. Similar research was conducted by Afefy and El-Tony (2019) but using combined post-installed FRP rods in shear and glass fiber-reinforced polymer (GFRP) sheets in flexure. Lapi et al. (2018) used a bonded reinforced concrete overlay when the flexural strengthening with FRP was not enough to achieve the design punching capacity. This technique augmented both the shear and flexural shear strength of existing slab–column connections. While flexural and punching shear strengths increase due to the greater slab thickness, the former increases further with the added tension reinforcement in the concrete overlay. However, roughening the existing concrete surface and using mechanical connectors are required to prevent premature debonding of the concrete overlay.

Engineered cementitious composites (ECC) are known for their capacity to experience tensile strain hardening, distribute cracks, and demonstrate excellent workability, rendering them a valuable material for enhancing structural strength. There is a significant interest in hybrid systems that combine ECC with other materials to optimize structural reinforcement and in advanced application techniques that streamline the integration process with existing structures. These studies are vital to maximizing the potential of ECC, mainly for strengthening flat slabs against punching shear.

Ultra-high-performance concrete (UHPC) is known for its very high compressive and tensile strengths compared to normal concrete, with innovative application applications, especially for shear enhancement (Chen et al., 2022, 2023; Li et al., 2023; Su et al., 2020). This strength is accompanied by a dense matrix and high fiber reinforcement, contributing to its exceptional durability and longevity. Limited research was carried out to assess the punching shear capacity of flat slabs constructed only using ECC or UHPC. These studies concluded that the fracture strength of ECC and UHPC has a significantly greater effect on the punching shear strength of slabs than the ultimate flexural strength (Joh et al., 2008; Lampropoulos et al., 2023; Zhou et al., 2020). Furthermore, recent research (Hou et al., 2020; Kadhim et al., 2021; Kim et al., 2021; Yehia et al., 2023; Zohrevand et al., 2015) has demonstrated that the utilization of UHPC and ECC for strengthening concrete enhances resistance against cracking and punching shear, resulting in a shift from brittle to ductile failure modes. This transformation improves overall structural performance (Hamoda et al., 2023b). Elsayed et al. (2022) employed ultra-high-performance fiber concrete (UHPFC) overlay to improve the punching shear strength of slab–column connections. They concluded that the strengthened slabs had significantly increased punching shear resistance and pre- and post-cracking stiffness.

The literature has shown a keen interest in using ECC and UHPC to repair concrete structures in composition with other strengthening materials against shear failure. However, combining ultra-high-performance concrete layers with shear dowels to augment the punching shear performance is as yet unavailable. This study experimentally and numerically addressed the efficiency of ultra-high-performance engineered cementitious composites (UHP-ECC) and Ultra-High-Performance Steel-Fiber-Reinforced Concrete (UHP-SFRC) as a viable option for retrofitting. UHP-ECC and UHP-SFRC were employed as a bonded concrete layer on the compression side of the slab around the column as indirect flexural strengthening and galvanized threaded steel bolts as direct shear strengthening through slab thickness to augment the punching shear strength. This technique allows for a significant increase in both the punching and flexural shear strength of existing slab–column connections. While both punching and flexural strengths increase owing to the larger thickness of the RC slab, the former expects to upgrade further with the added compression reinforcement in the UHP layer. A series of tests are carried out and reported in this study. A numerical model is also developed and verified using the test data.

2 Experimental Program

2.1 Test Program and Specimen Details

The test matrix included six square flat slabs with central circular columns that were constructed and tested to collapse at the Kafrelsheikh University in Egypt. The width and thickness of the slabs were 1000 mm and 100 mm, respectively. The tension steel reinforcement was taken as D10 at 200 mm spacing in each direction, while the compression steel reinforcement was D8 at 200 mm spacing in each direction, as depicted in Fig. 1a. A circular column of 100 mm diameter was cast at the slab center, simulating an interior slab–column region in a

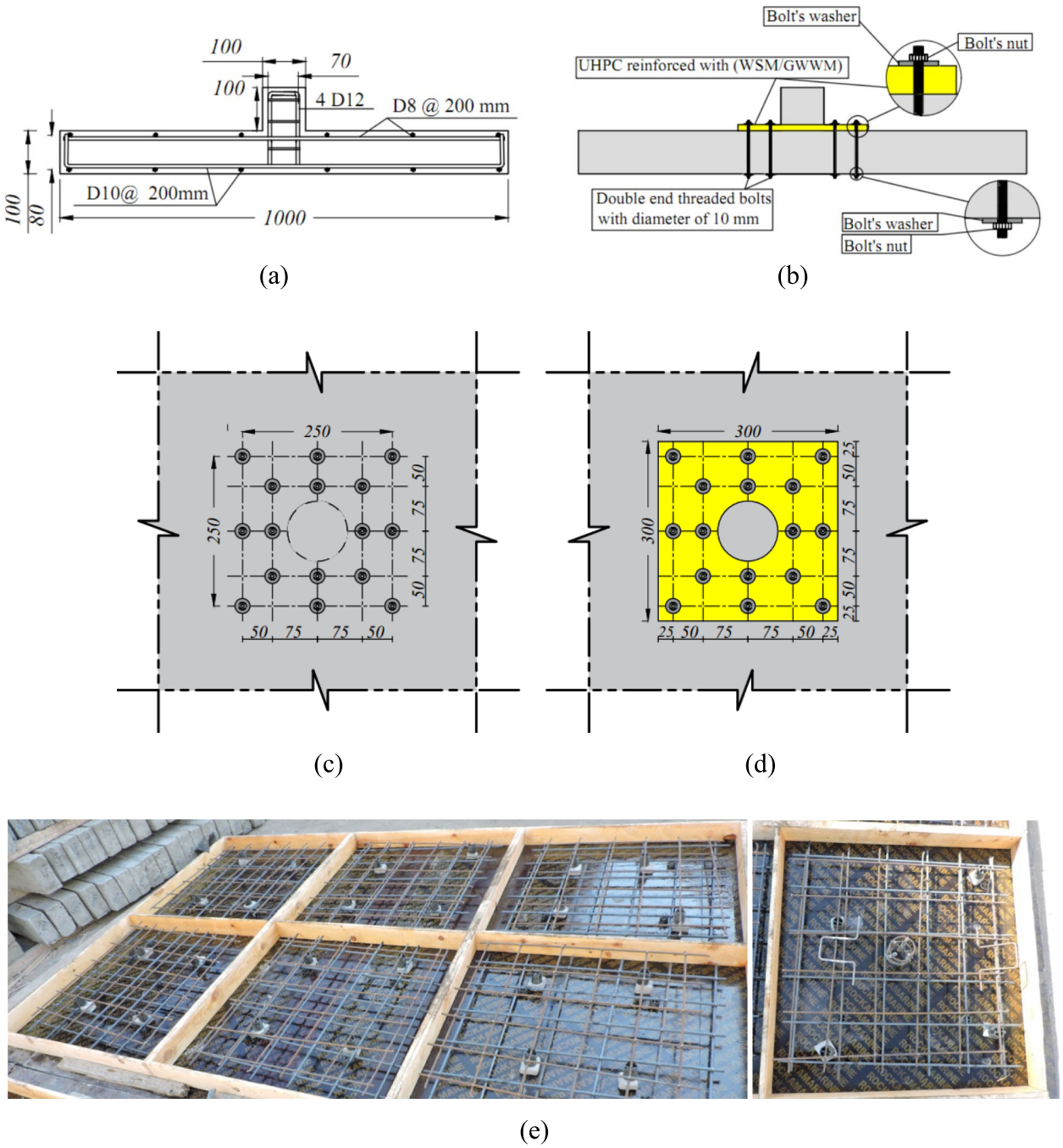

Fig. 1 Description of the tested RC slabs: **a** reinforcement details of the slabs; **b** strengthening details; **c** view of the bottom surface with steel threaded bolt arrangement around the column; **d** view of the slab's top surface showing bolt arrangement and the UHPC layer; **e** photos of the formwork and reinforcement. (Units in mm)

flat slab floor. The first slab, S, was considered as the unstrengthened control specimen. The other five slabs were strengthened in flexure by casting a UHPC layer of 10 mm thickness on the compression side of the slab, as depicted in Fig. 1b and c. Steel bolts with washers and nuts were installed per the arrangement in Fig. 1b and c to provide the required bond between the UHPC layer and the existing concrete and to enhance the punching capacity. The width of the strengthening layer was estimated according to the width of the drop panel recommended by ACI 318–19 (2019) (i.e., $l/3 = 300\ mm$).

The first slab group included the control specimen, S which has been set from the previous study carried out by Hamoda et al. (2024d). This group also consists of two identical specimens, S-Wr-UE, and S-Wr-US, strengthened with UHP-ECC and UHP-SFRC layers, respectively, along with galvanized welded wire mesh (GWWM). The second slab group was similar to the first group except that the GWWM mesh was replaced with welded steel mesh (WSM). The second group included a fourth specimen, S-Wd-Wr-UE, that was strengthened with a UHP-ECC layer with two reinforcement meshes; the first reinforcement layer was steel welded wire (SWM) mesh, while the second layer was galvanized welded wire mesh (GWWM). This was in addition to the threaded bolts as in other strengthened slabs. Table 1 summarizes the slab details.

2.2 Material Properties

This study employed three concrete mixtures: normal concrete (NC), UHP-ECC, and UHP-SFRC. The conventional concrete has been delivered with the mix proportion tabulated in Table 2. The flowable UHP-ECC was a mix of fine aggregate, polypropylene (PP) fiber, Portland cement, silica fume, high-range water reducer, and admixtures. The respective water-to-binder ratio was 0.27, achieved through mixing in a mechanical horizontal shear mixer. This UHP-ECC was prepared with respect to the mix proportion shown in Table 2. The flowable UHP-SFRC incorporated fine aggregate, steel fiber, silica fume, Portland cement, high-range water reducer, and admixtures. The water-to-binder ratio (w/b) of 0.2 was used. The UHP-SFRC composition per cubic meter was 850 kg cement, 1030 kg fine aggregates, 200 kg silica fume, 2% steel fibers by weight, and 28 kg high-range water reducer.

These concrete cylinders were cast concurrently with the slabs and underwent curing in identical room conditions. The concrete compressive strength was calculated by averaging the test outcomes of three 150 × 300 mm concrete cylinders. The average compressive strength

Table 1 Test matrix

Group	Slab's ID	Identical details		Details of punching zone's strengthening	
		Slab's type	Reinforcement	Reinforcement type	Type of HPC
G1	S (Hamoda et al., 2024d)	Conventional concrete with $f_c' = 32$ N/mm^2	- Compression: 6 #8 - flexural: 6 #10	–	–
	S-Wr-UE			GWWM	UHP-ECC
	S-Wr-US			GWWM	UHP-SFRC
G2	S (Hamoda et al., 2024d)			–	–
	S-Wd-UE			WSM	UHP-ECC
	S-Wd-US			WSM	UHP-SFRC
	S-Wd-Wr-UE			WSM + GWWM	UHP-ECC

GWWM galvanized welded wire mesh, *WSM* welded steel mesh

Table 2 Mix proportion

Concrete	Cement with 52.5R (kg/m^3)	Fine aggregate (kg/m^3)	Coarse aggregate (kg/m^3)	Fly ash (kg/m^3)	Silica fume (kg/m^3)	W/b	PP or SF (%)	HRWR (kg/m^3)
NC	355	698	1143	–	–	0.42	–	–
UHP-ECC	800	500	–	750	150	0.27	2%	40 (S.P.)
UHP-SFRC	850	1030	–	–	200	0.2	2%	28

Cement grade 52.50 N/mm^2, W/b: water-to-bender ratio (bender = cement, fly ash, and silica fume), PP: polypropylene fiber, SF: steel fiber, HRWR: high-range water reducer, S.P.: superplasticizer

was 32 N/mm^2 for normal concrete used to cast the slabs, 129 N/mm^2 for UHP-ECC, and 141 N/mm^2 for UHP-SFRC. Table 3 shows the mechanical properties of NC, UHP-ECC, and UHP-SFRC obtained experimentally that have been employed for numerical investigation. The tensile stress–strain response of NC, UHP-ECC, and UHP-SFRC was determined by subjecting dog-bone-shaped test specimens to uniaxial tension.

Samples were tested under tensile force to collapse to acquire the mechanical properties of the reinforcing steel bars D8, D10, and D12. The D8 steel bars exhibited yield and ultimate tensile strengths of 280 and 360 MPa, respectively, while these values were 354 MPa and 410 for the D10 bars. The D12 steel bars demonstrated measured yield and ultimate tensile strengths of 352 and 415 MPa, respectively. The galvanized welded wire (GWWM) mesh had the yield and ultimate tensile strengths of 240 and 310 MPa, respectively. The GWWM had an opening size of (10×10) mm^2 size with a diameter of 0.5 mm, as shown in Fig. 2 (h). The welded steel (WSM) mesh had the yield and ultimate tensile strengths of 275 and 355 MPa, respectively. The WSM had an opening size of (40×40) mm^2 with a bar diameter of 3 mm, as shown in Fig. 2 (h). Threaded bolts used to strengthen the slab in shear were of 10 mm diameter with 382 and 423 MPa for yield and tensile strength, respectively. Table 4 summarizes the mechanical properties of the reinforcement that has been employed in the numerical section.

2.3 Casting and Preparation for Strengthening

The steel reinforcement was placed in the bed of the formworks prepared for casting the slabs, as depicted in Fig. 1e, before normal concrete casting. After concrete hardening, strengthening was implemented in five tested slabs. First, the existing concrete compression surface was roughened over a 300 mm by 300 mm slab area around the column to increase shear friction resistance between the existing concrete and the UHPC layer. Second, holes were drilled through the slab thickness per the arrangement of post-installed bolts in Fig. 1c, as shown in Fig. 2a. However, the bolts were slightly repositioned from their locations to avoid interference with the steel bars. Then, air pressure was used to remove dust from the holes and the concrete surface. Threaded bolts were then assembled into the drilled holes employing chemical adhesive epoxy to augment the bond between the bolts and the existing slab. As depicted in Fig. 2c and d, the WSM reinforcement layer was placed followed by casting a portion of UHPC. In the last slab, two layers of reinforcement were placed in the form, before casting UHPC. After UHPC hardening, washers, and nuts were used to secure the steel bolts in position by tightening the nuts. This would help prevent premature debonding of the overlaid UHPC under load. Before testing commenced, all beams were cleaned and whitely coated to improve visibility and facilitate crack identification during testing.

2.4 *Test Setup* and Procedure

A high-capacity crane was employed to handle, move, and level the slabs over the supports to prepare the test setup. Figure 3a presents a schematic representation of the test setup, while Fig. 3b shows a photo before testing. Each slab was positioned over line supports at its four sides. A single linear variable displacement transducer (LVDT) was used to record the vertical deflection at the slab center, as illustrated in Fig. 3. Four PI gauges were placed on the tension side of the slab at the edges of UHPC, as illustrated in Fig. 3c and d to measure both the first cracking width and tensile strains under load. The slabs were gradually loaded in increments until failure, with any visible cracks marked and deflection readings logged using a data logger at each load step. Just before the failure occurred, the LVDT was disengaged. However, to better demonstrate the punching of the circular column beyond the ultimate load and failure, the jack was lowered to clearly display the penetration.

3 Test Results and Discussion

3.1 Deformed Shape and Failure Mode

The crack pattern and failure mode of the unstrengthened control slab, S, is shown in Fig. 4. The first flexural crack appeared at the slab center under the column at 38 kN load. With the increase in load, radial cracks resulting from tangential moments disperse from the perimeter of the load location, breaking the slab into a fan-like fashion. As the load kept increasing, the crack widths

Table 3 Concrete properties

Concrete	Compression			Tension		
	$f_{c'}$ (N/mm^2)	*Strain at* $f_{c'}$	Maximum strain	f_t (N/mm^2)	*Strain at* f_t	Maximum strain
NC	32	0.002	0.003	2.76	0.0002	0.015
UHP-ECC	129	0.001	0.012	11.85	0.003	0.06
UHP-SFRC	141	0.0064	0.045	12.15	0.0002	0.015

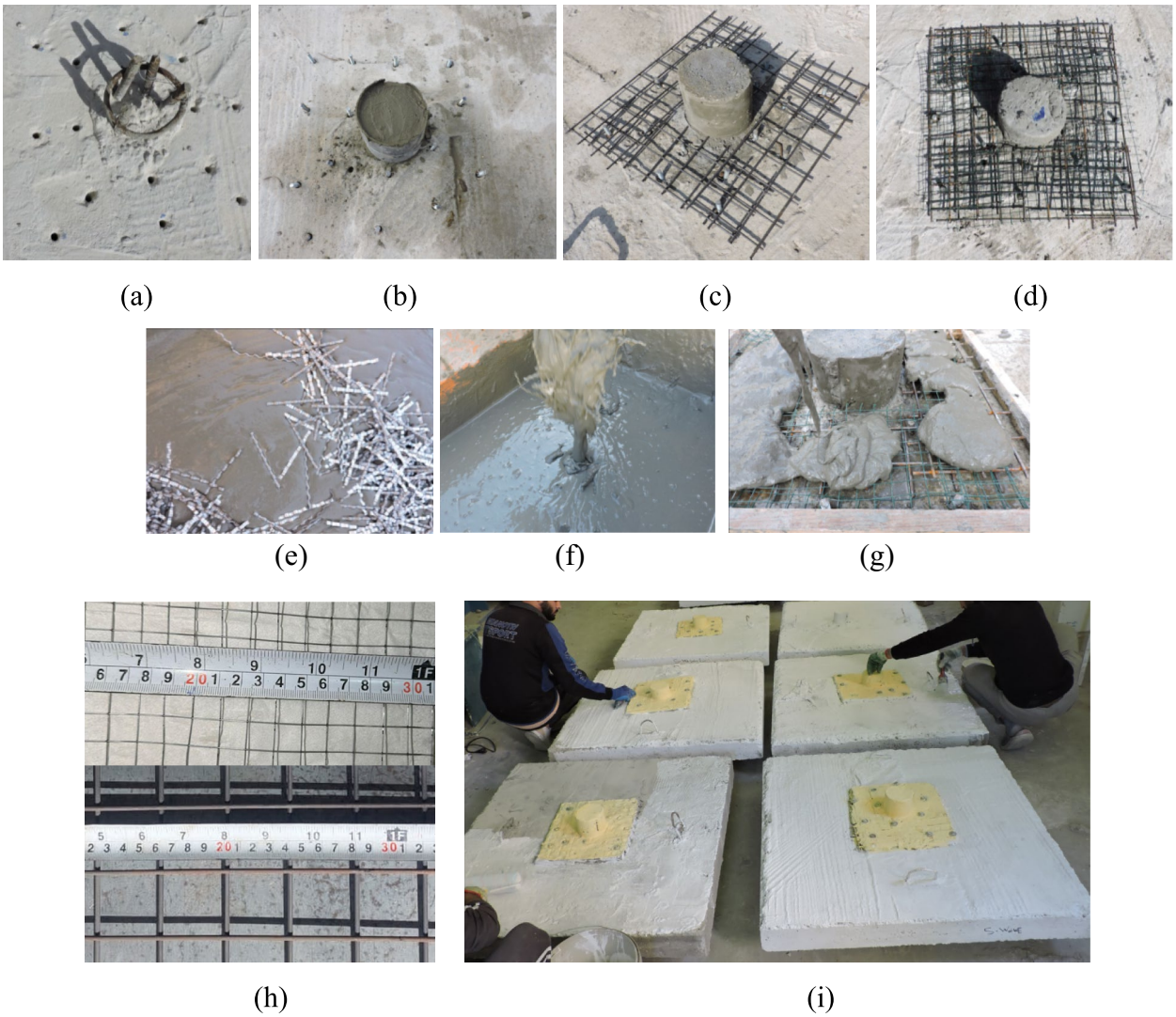

Fig. 2 Strengthening arrangement: **a** arrangement and positioning of the double-end threaded bolts; **b** post-casting of the circular column; **c** positioning of the WSM mesh; **d** WSM in addition to GWWM mesh; **e** steel fiber used for UHP-SFRC; **f** flowable UHP-SFRC; **g** casting of UHP-ECC; **h** GWWM and WSM, and **i** installing bolts and painting of slabs before testing

Table 4 Reinforcement properties

Steel element	Presence	Yield stage		Ultimate stage		E (GPa)	Poisson's ratio
		σ_y (MPa)	ε_y (%)	σ_u (MPa)	ε_u (%)		
8 mm	Compressive steel	280	0.141	360	11.98	200	0.30
10 mm	Flexural steel	354	0.179	410	12.23	197	0.30
12 mm	Column steel	352	0.172	415	14.01	206	0.30
GWWM	Strengthening	240	0.141	310	12.25	170	0.30
WSM	Strengthening	275	0.138	355	10.79	200	0.30
Threaded bolts	Connector	382	0.189	423	11.45	203	0.30

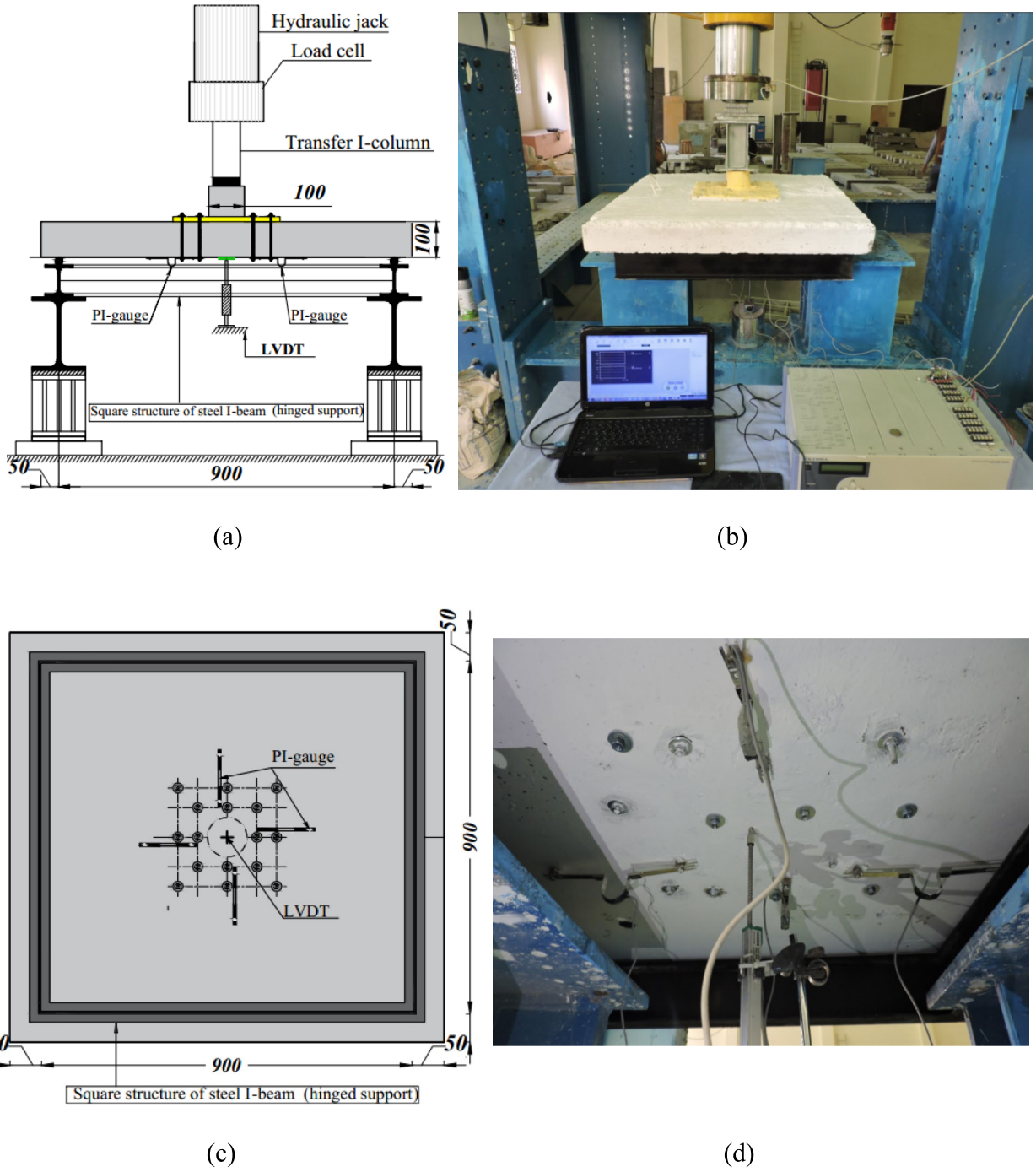

Fig. 3 Test setup and sensor locations: **a** schematic details of the test setup; **b** photo of the test setup; **c** schematic plan of the sensor locations; **d** photo of the attached sensors

increased with a few new cracks, and then punching shear failure occurred suddenly. Punching shear failure appeared through the column perforating into the slab top surface, and signs of concrete peeling or popping out along a significant portion of the bottom perimeter of the cone-shaped perforation, showing circumferential cracks, as depicted in Fig. 4.

In the second slab, S-Wr-UE, with combined strengthening using GWWM-reinforced UHP-ECC in the compression side and steel bolts through slab thickness, the

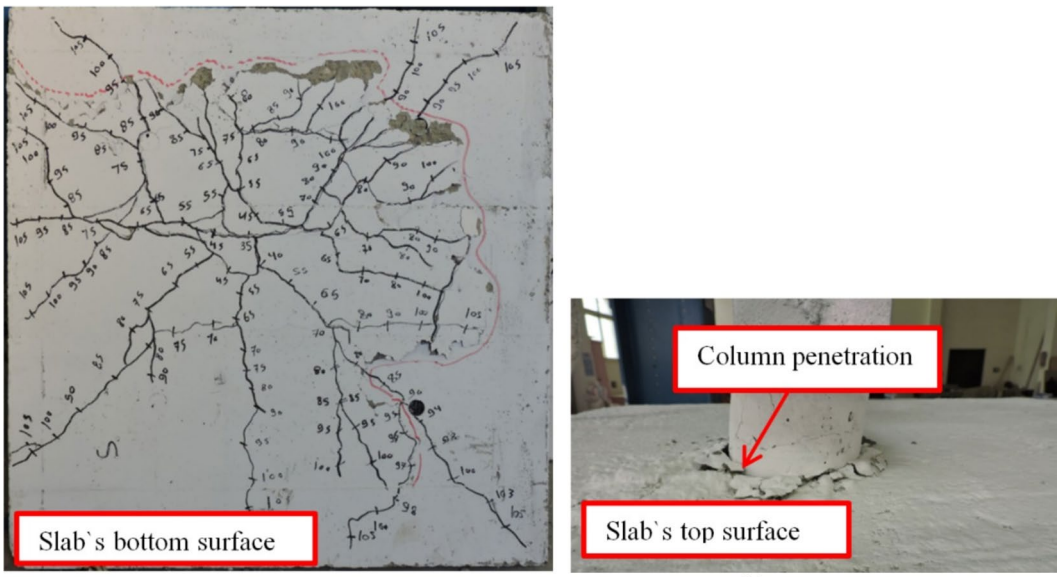

Fig. 4 Punching shear failure mode of the unstrengthened slab: **a** bottom view; and **b** top view. (image source: Hamoda et al. (2024d))

first flexural crack appeared on the slab's tension side at the load location at 45 kN load. This crack propagated outside the UHP-ECC region with increased applied load. Additional radial flexural cracks appeared in the NC slab outside the UHP-ECC overlay region. They extended towards the support lines with increased applied load until sudden punching shear failure outside the UHP-ECC area, along with extensive flexural cracks at the column location, occurred, as depicted in Fig. 5a.

Failure modes and crack patterns are shown in Fig. 5b for the third slab, S-Wr-US, with GWWM-reinforced UHP-SFRC layer and steel bolt strengthening. The first crack was observed at the tension side of the slab under the column at 55 kN load. With the increase in the applied load, this crack propagated toward the supports in a fan-shaped pattern. Then, sudden punching shear occurred, as depicted in Fig. 5b. Concrete spalling appeared on the tension side of the slab along a significant portion of the punching shear perimeter.

Figure 6a shows the fourth slab's crack pattern and failure mode, S-Wd-UE, with combined WSM-reinforced UHP-ECC and steel bolts. The first flexural crack was noticed under the column at 70 kN. The crack pattern was observed to be leading to punching shear failure, as depicted in Fig. 6a. The failure mode and crack pattern of the fifth slab, S-Wd-US, with WSM-reinforced UHP-SFRC and steel bolts is shown in Fig. 6b. After the initiation of flexural crack at 75 kN, radial flexural cracks appeared in an almost symmetrical fashion leading to failure due to punching shear.

Figure 6c shows the sixth slab's crack pattern and failure mode, S-Wd-Wr-UE, with UHP-ECC reinforced with two layers of steel meshes and steel bolts through slab thickness. The first flexural crack was observed under the column at 80 kN. The crack pattern was observed to be leading to punching shear failure, given the sudden drop in the applied load and the appearance of concrete spalling at the tension side of the slab along parts of the punching shear perimeter. However, signs of major visible wide cracks originating from the column location toward the support corners, as depicted in Fig. 6c, make the slab failure a combined flexural-punching type. At the end of each of the five tests, no signs of debonding of the UHPC layer were observed. In addition, no failure in the steel bolts was noted.

3.2 Loads, Elastic Stiffness, and Absorbed Energy

Table 5 summarizes the experimental findings obtained. The tested slabs exhibited punching shear failure except for the last slab, which failed due to combined flexure and punching shear. Comparing the second slab with the UHP-ECC layer, and the third slab with the UHP-SFRC layer, one may observe that the cracking load increased by 18% and 45%, respectively, compared to the control slab. In addition, comparing the second slab with the UHP-ECC layer and the third slab with the UHP-SFRC layer, one may observe that the peak load increased by 29% and 65%, respectively, over that of the control slab. Given their mechanical properties, one may conclude that the UHP-SFRC exhibited better performance than

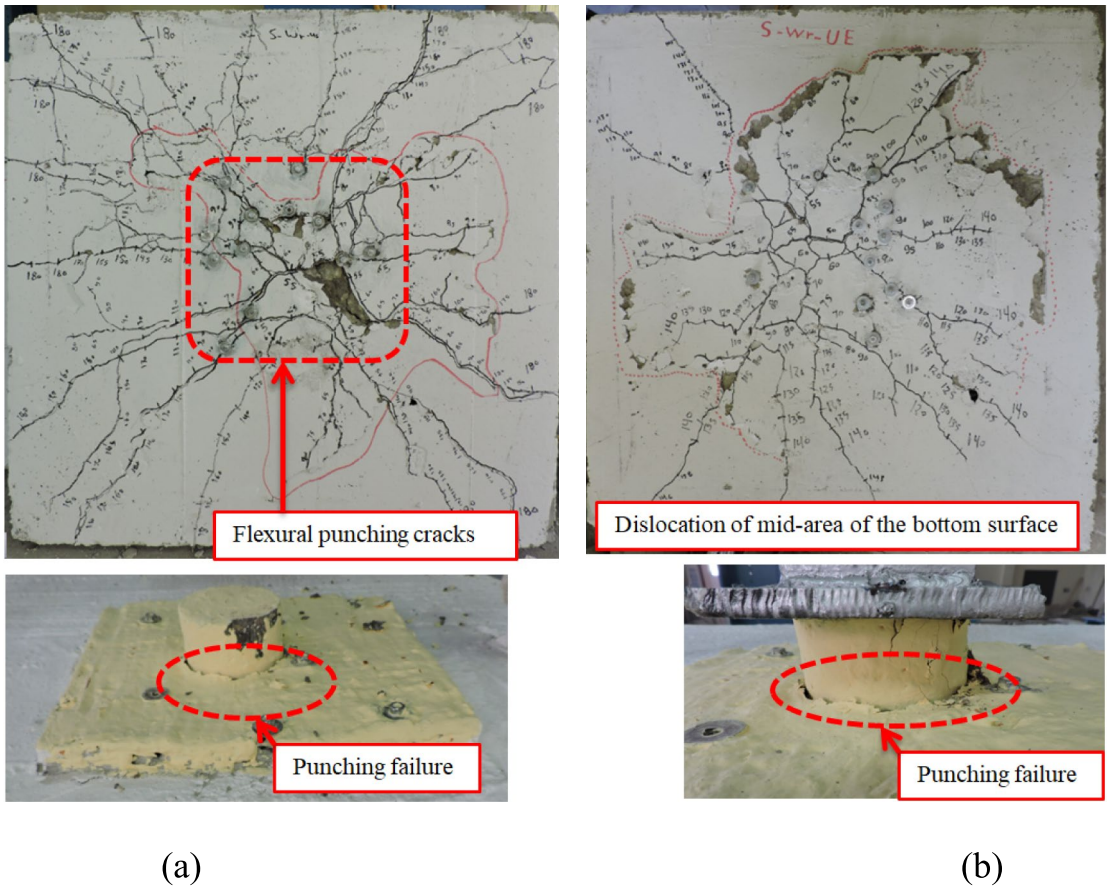

Fig. 5 Crack patterns and failure modes of slabs of the first group: **a** S-Wr-UE slab; and **b** S-Wr-US slab

the UHP-ECC. However, the change in the type of UHPC did not alter the failure mode, which was punching shear.

Similar behavior was observed in the case of the fourth and fifth slabs of group 2 that were reinforced with WSM mesh instead of GWWM mesh, except that the UHPC layer has a more significant effect than the master slab. Comparing the fourth and fifth slabs with UHP-ECC and UHP-SFRC layers increased the cracking load by 84% and 97%, respectively, larger than the ordinary slab. In addition, comparing the fourth slab with the UHP-ECC layer and the fifth slab with the UHP-SFRC layer, the resistance force was enhanced by 62% and 100%, respectively, over that of the control slab.

When comparing the sixth slab with two layers of reinforcement in the UHP-ECC layer with the fifth slab with only one layer of reinforcement, one may notice that the cracking and ultimate loads increased by 7.1% and 5.5%, respectively, compared to the control specimen. Although the increase in the crack and ultimate loads were insignificant, the failure mode shifted from punching shear to combined flexure and punching shear. They may be attributed to increased flexural strength locally around the column using the UHP-ECC strengthening layer, delaying the sudden punching shear failure to a greater applied load level. Table 5 reports the deflection and crack width at the first crack stage, along with the deflection at the failure load. While these parameters are important, an insignificant change in these values was observed with the change in the strengthening technique compared to the control specimen.

As an indication of the elastic and plastic performance of the tested slabs, elastic stiffness (K) and absorbed energy (AE) were calculated, as shown in Table 5. The K value was computed as the slope of linear response up to the crack load, while the AE value was estimated as the total area under load–deflection response up to the peak load. Results in Table 5 showed that strengthening the slab with the UHP-ECC layer and UHP-SFRC layer in the compression side of the slabs with post-installed bolts increased the elastic stiffness by 1.65 and 1.41 times, respectively, compared to the unstrengthened slab in slab group 1. Corresponding values of 1.2 and 1.6 times were observed for the fourth and fifth specimens in slab group 2. A similar trend was noted in the case of

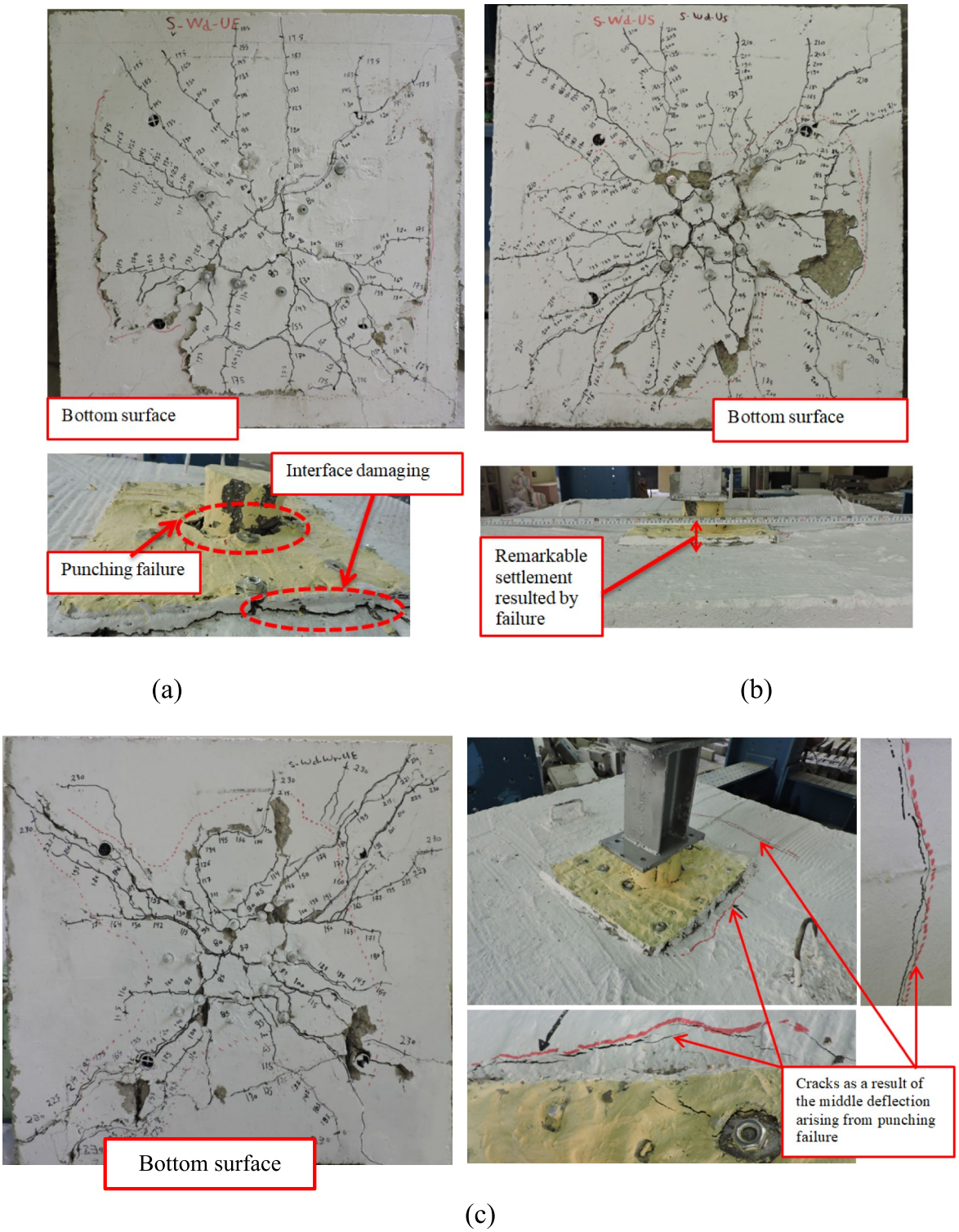

Fig. 6 Crack patterns and failure modes of slabs of the second group: **a** S-Wd-UE slab; **b** S-Wd-US slab; and **c** S-Wd-Wr-UE slab

the absorbed energy reaching ultimate capacity, as it was enhanced by 109% and 161% for both the second and third slabs, respectively, compared to the control slab. These enhancements were 175% and 227% in the case of the fourth and fifth slab specimens, respectively. One may observe that the slabs strengthened with WSM mesh

Table 5 Experimental test results

Group	Name	Cracking stage				Ultimate stage			Elastic stiffness (K)		Absorbed energy (AE)		Failure mode
		P_{cr} (kN)	P_{crS}/P_{crS0}	w_{cr} (mm)	Δ_{cr} (mm)	P_u (kN)	P_{uS}/P_{uS0}	Δ_{Pu} (mm)	K	K_S/K_{S0}	AE	AEs/AEs0	
G1	S (Hamoda et al., 2024d)	38	1.00	0.2	9.50	110	1.00	25.8	4.02	1.00	1380	1.00	Punching
	S-Wr-UE	45	1.18	0.20	4.25	140.35	1.29	31.28	10.59	2.65	2878.75	2.09	Punching
	S-Wr-US	55	1.45	0.19	5.69	181.40	1.65	32.97	9.66	2.41	3600.94	2.61	Punching
G2	S (Hamoda et al., 2024d)	38	1.00	0.20	6.28	10,842	1.00	29.01	5.27	1.00	1379	1.00	Punching
	S-Wd-UE	70	1.84	0.20	7.97	175.23	1.60	34.78	8.78	2.20	3796.15	2.75	Punching
	S-Wd-US	75	1.97	0.20	7.04	217.37	2.00	44.76	10.59	2.66	4508.18	3.27	Punching
	S-Wd-Wr-UE	80	2.11	0.18	8.85	228.90	2.10	42.92	9.04	2.26	6057.12	4.39	flexure + punching

outperformed those strengthened with GWWM mesh due to the difference in their mechanical properties mentioned earlier.

3.3 Load–Deflection Relationships

The load–displacement curves for all experimented slabs are presented in Fig. 7. Results in Fig. 7 show that all slabs displayed a bilinear behavior through two phases up to the ultimate load. The first phase is characterized by the initial flexural stiffness of the uncracked concrete at the early loading stage. In contrast, the second phase is characterized by reduced flexural stiffness because of the formation of flexural cracks. Beyond the peak stage, the unstrengthened slab that experienced primary punching shear collapse had a sudden drop in the load while maintaining an almost linear load–deflection relationship before failure. The second and third slabs reinforced with UHP-ECC and UHP-SFRC experienced a similar failure mode and sudden drop in load after experiencing a slight reduction in flexural stiffness before failure, as depicted in Fig. 7a. This means that the failure of these two slabs was brittle. Corresponding fourth and third slabs with different steel mesh types showed a similar trend, as depicted in Fig. 7b.

4 Numerical Simulation

The finite-element method (FEM) is known as a valuable tool for researchers to predict the structural behavior of concrete elements in a cost-effective and time-saving way. This study utilizes ABAQUS software to develop a 3D-FE model replicating the performance of tested slabs. A thorough validation process was conducted to ensure the FE model's accuracy, comparing its results to the corresponding experimental data.

4.1 Details of the Finite-Element Modeling

To precisely replicate the experimental setup, a detailed FEM model of the tested slabs was developed as depicted in Fig. 8. The model employed a specific element type, eight-node linear reduced integration solid elements (C3D8R), to accurately represent normal concrete, UHP-ECC, and UHP-SFRC. This model has been used herein and can significantly cut down computational time and resources. Moreover, full integration elements can suffer

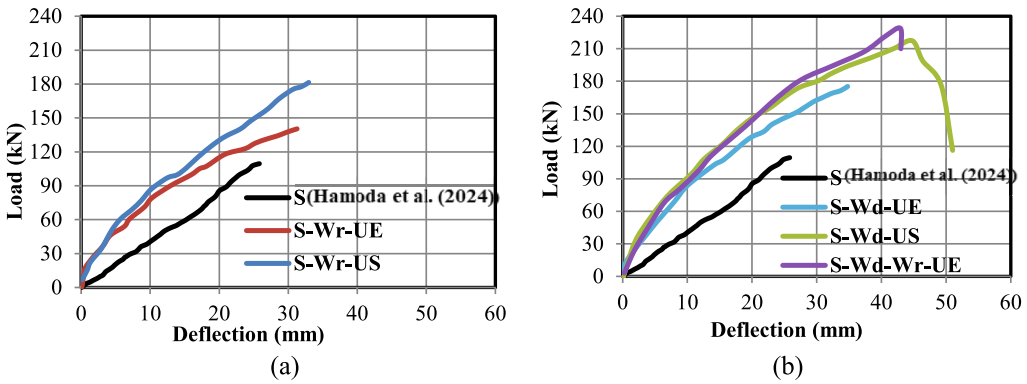

Fig. 7 Load–deflection curves for the tested slabs: **a** the first group and **b** the second group

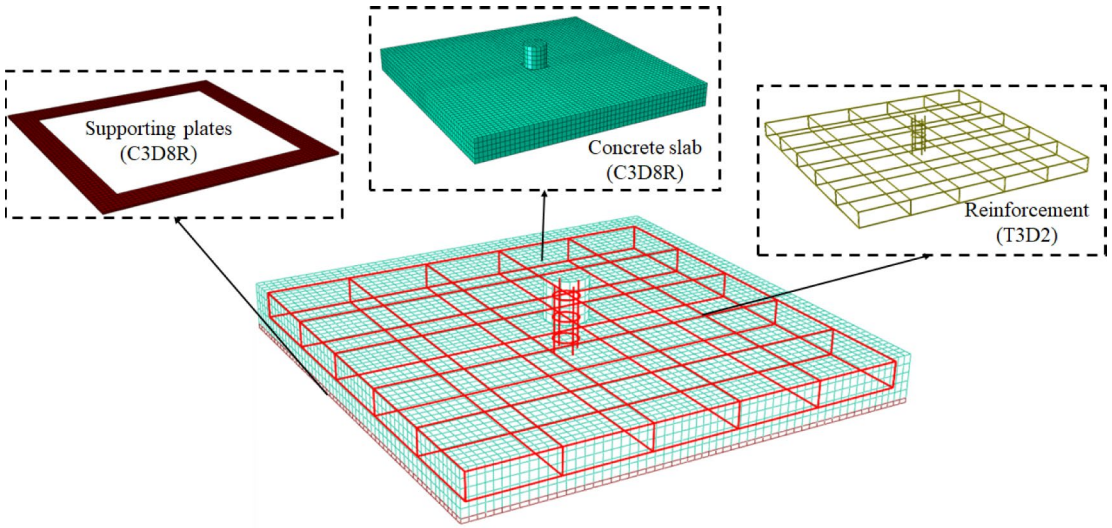

(a)

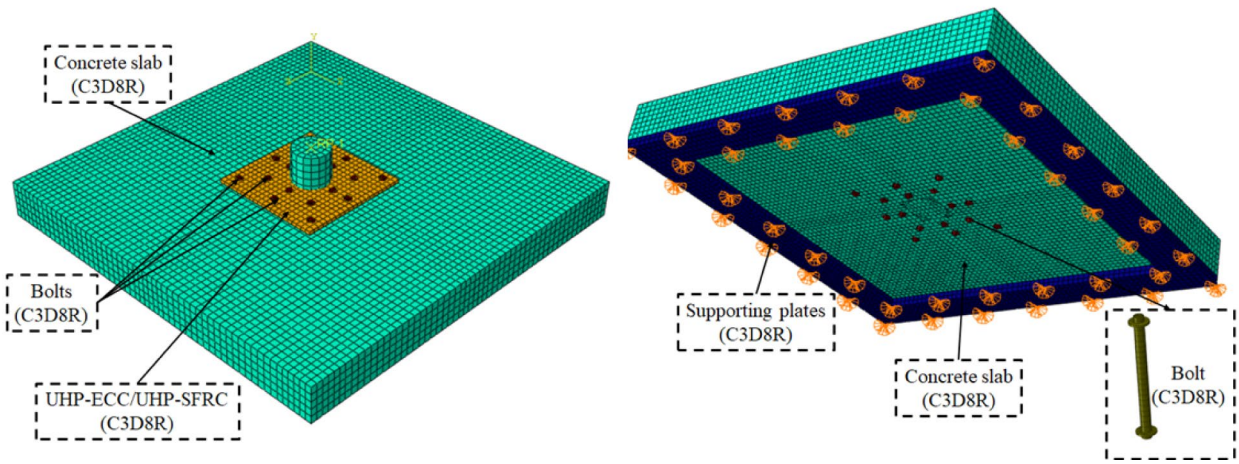

(b)

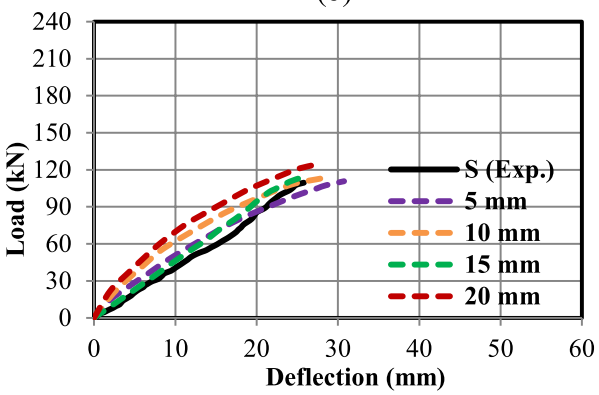

(c)

Fig. 8 Views of the finite-element model: **a** slab reinforcement, **b** strengthened slab and, **c** sensitivity analysis of mesh size

from volumetric locking, especially with materials such as UHP-ECC and UHP-SFRC, and reduced integration elements help mitigate this issue. In addition, previous studies carried out by Hamoda et al., (2024a, 2024c, 2024d, 2025) have shown that C3D8R elements can accurately capture the behavior of concrete and similar materials with proper mesh refinement and calibration. This same element type was also used to model the loading and supporting plates, along with the steel bolts connecting the UHPC layer to the slab. For computational efficiency, all steel bars were simulated with a different element type: two-node linear 3D truss elements (T3D2), as illustrated in Fig. 8. T3D2 elements kept the focus on the axial load-bearing characteristics. It provides computationally less demanding than three-node beam elements, allowing for faster simulations, especially for large-scale models. Beam elements introduce complexities related to bending and shear deformations, which were not the focus of this study. Previous studies confirmed the less computational cost for the T3D2 model (Eltaly et al., 2024; Hamoda et al., 2024e, 2024f). Finally, the GWWM and WSM reinforcement layers were simulated using four-node, quadrilateral shell elements with reduced integration (S4R). S4R elements exhibit less sensitivity to element distortion compared to Q3 elements. This characteristic is particularly crucial when addressing complex geometries and meshing difficulties, commonly found in reinforced concrete structures. In addition, S4R elements are less susceptible to shear locking, a numerical issue that can result in inaccurate outcomes, especially for thin shell elements. The model meticulously replicates the loading conditions to reflect the real-world experiment accurately. A reference point, securely attached to the column's top surface, applies the load through a coupling constraint. This approach mimics the experimental setup, where a similar connection applied the force. Furthermore, just as the supporting plates were restrained in the experiment, the model restrained them against vertical movement.

The finite-element model employed two key approaches to realistically simulate the interactions between the various components of the slab. A "bond behavior" was simulated through an embedded region constraint to represent the bond between the steel reinforcement (i.e., bars and mesh) interacting with the surrounding concrete. The steel bars were fully integrated into the slab body using an embedded element condition, with the steel bars acting as the host region within the slave NC slab type. Such an approach treats the concrete as the primary structure with the embedded steel elements. This accurately reflects how well the steel adheres to the concrete, a crucial factor in the slab's performance. The interface interaction was simulated using a surface-to-surface contact approach to model the interaction between the slab-UHP-ECC and UHP-SFRC layers. A coefficient of 0.6 was applied in the tangential direction to account for the sliding resistance between the two materials based on the previous recommendations (Hamoda et al., 2023a, 2023c, 2024b). A "hard contact" behavior was assumed in the normal direction, meaning the surfaces cannot interpenetrate. A perfect bond was also assumed between the concrete slab and the loading and supporting plates.

4.2 Constitutive Modeling of Materials

To represent the complex behavior of NC, UHP-ECC, and UHP-SFRC under load, the concrete damage plasticity (CDP) model was employed. This versatile model effectively simulates these diverse concrete compressive and tensile responses. For NC, a well-established stress–strain relationship developed by Carreira and Chu (1985), calculated using Eqs. 1 to 3, was incorporated into the simulations. For both UHP-ECC and UHP-SFRC, the stress–strain relationships were developed based on the work of Zhou et al. (2015) using Eqms. 4 and 5. For steel elements, a linear elastic–plastic material model with strain hardening was utilized to represent steel in the modeling:

$$f_c = f_c' \left[\frac{\beta\left(\frac{\varepsilon_c}{\varepsilon_{c0}}\right)}{\beta - 1 + \left(\frac{\varepsilon_c}{\varepsilon_{c0}}\right)^{\beta}} \right] \tag{1}$$

$$f_t = \begin{cases} f_{tu}\left[1.2\frac{\varepsilon_t}{\varepsilon_{t0}} - 0.2\left(\frac{\varepsilon_t}{\varepsilon_{t0}}\right)^6\right] 0 \le \varepsilon_t \le \varepsilon_{t0} \\ f_{tu}\left[\frac{\frac{\varepsilon_t}{\varepsilon_{t0}}}{1.25\left(\frac{\varepsilon_t}{\varepsilon_{t0}}-1\right)^2 - \frac{\varepsilon_t}{\varepsilon_{t0}}}\right] \varepsilon_{t0} \le \varepsilon_t \end{cases} \tag{2}$$

where f_c and ε_c represent the stress and strain of the concrete material, respectively. The variables f'_c and ε_{co} correspond to the peak compressive strength and its associated strain, respectively. Furthermore, the β factor can be determined using Eq. (3), which was derived based on the stress–strain depiction:

$$\beta = \left(\frac{f_c'}{32.4}\right) + 1.55 \tag{3}$$

$$f_c = \begin{cases} E_0\varepsilon_c & \varepsilon_c \le 0.4\varepsilon_{cp} \\ E_0\varepsilon_c\left(1 - 0.308\frac{E_0\varepsilon_c}{f_c'} + 0.124\right) & 0.4\varepsilon_{cp} < \varepsilon_c \le \varepsilon_{cp} \end{cases} \quad (4)$$

$$f_t = \begin{cases} \frac{f_{tc}}{\varepsilon_{tc}}\varepsilon_t & 0 \le \varepsilon_t \le \varepsilon_{tc} \\ f_{tc} + \frac{f_{tu}-f_{tc}}{\varepsilon_{tu}-\varepsilon_{tc}}(\varepsilon - \varepsilon_{tc}) & \varepsilon_{tc} \le \varepsilon_t \le \varepsilon_{tu} \end{cases} \quad (5)$$

where both E_0 and εcp represent Young's modulus of ECC, and maximum linear strain, respectively; f_{tc} and ε_{tc} denote the tensile strength of ECC, and strain at the initial crack, respectively; f_{tu} and ε_{tu} refer to ultimate tensile capacity with its strain, respectively.

A sensitivity study calibrated its key parameters to ensure that the concrete damaged plasticity (CDP) model accurately reflects concrete exhibition. This analysis revealed that the angle of dilatation (ψ) played a critical role in distinguishing between NC, UHP-ECC, and UHP-SFRC. NC exhibited a ψ value of 25 degrees, while UHP-ECC and UHP-SFRC required a slightly higher value of 30 degrees for proper behavior representation. Following ABAQUS software guidelines, other CDP model parameters were assigned specific values: eccentricity flow potential (e) = 0.1, biaxial to uniaxial compressive strength ratio (f_{b0}/f_{c0}) = 1.16, ratio (K_c) = 0.667, and viscosity parameter (μ) = 0.0001. Beyond calibrating the model's parameters, achieving an optimal balance between accuracy and computational efficiency was critical. This involved optimizing the mesh size used in finite-element modeling. Figure 8(a) presents a parametric sensitivity analysis of the mesh size, which varies from 5 to 20 mm. Smaller mesh sizes resulted in higher computational costs, while larger mesh sizes produced unacceptable results. Consequently, the study identified a mesh size of 15 mm as providing an economical solution with acceptable results. The number of mesh nodes, together with mesh numbers, are provided in Table 6. These data are crucial for understanding the structural analysis and computational modeling of the components. Table 6 provides detailed information on various components of a structure, including a concrete slab, a strengthening layer, steel bars, GWWM/WSM, and bolts. It lists the number of nodes and elements for each component, with the concrete slab having the highest number of nodes (19,771) and elements (15,980). The bolts have the highest number of nodes (42,384) and elements (26,144), indicating a complex and detailed mesh for these components.

4.3 FEM Verification

To ensure the accuracy of the FEM, rigorous validation was conducted by comparing them against experimental findings, as depicted in Fig. 9. This comparison focused on the load–deflection relationship, a key indicator of slab behavior under stress. The FEM reasonably captured the overall behavior at all loading stages, demonstrating their ability to represent the true structural response of the slabs accurately.

Table 6 Number of meshes and nodes

Component	Concrete slab	Strengthening layer	Steel bars	GWWM/WSM	Bolts
No. of nodes	19,771	968	1359	896	42,384
No. of elements	15,980	441	1331	392	26,144

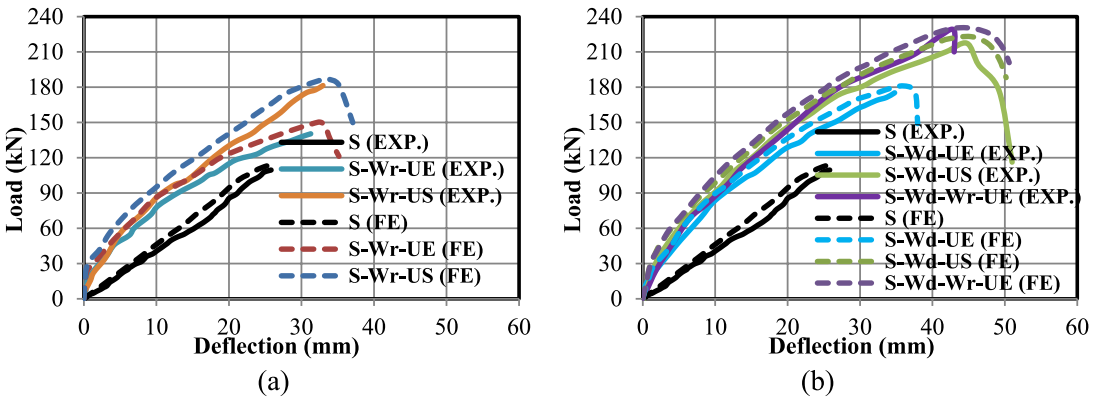

Fig. 9 Load–deflection curves obtained from the FE modeling and experiments for the tested slabs: **a** the first group; and **b** the second group

Table 7 Experimental versus FE results

Name	Cracking stage						Ultimate stage					
	$P_{cr,FE}$ (kN)	$P_{cr,EXP}$ (kN)	$P_{cr,FE}/P_{cr,EXP}$	$\Delta_{cr,FE}$ (mm)	$\Delta_{cr,EXP}$ (mm)	$\Delta_{cr,FE}/\Delta_{cr,EXP}$	$P_{u,FE}$ (kN)	$P_{u,EXP}$ (kN)	$P_{u,FE}/P_{u,EXP}$	$\Delta_{u,FE}$ (mm)	$\Delta_{u,EXP}$ (mm)	$\Delta_{u,FE}/\Delta_{u,EXP}$
S (Hamoda et al., 2024d)	40	38	1.05	9.1	9.5	0.99	114.5	110	1.04	26.3	25.8	1.02
S-Wr-UE	48	45	1.07	6.83	4.25	1.61	150.29	140.35	1.07	32.55	31.28	1.04
S-Wr-US	57	55	1.04	8.92	5.69	1.57	186.93	181.40	1.03	33.61	32.97	1.02
S-Wd-UE	72	70	1.03	9.14	7.97	1.15	181.06	175.23	1.03	36.04	34.78	1.04
S-Wd-US	78	75	1.04	9.87	7.04	1.40	223.03	217.37	1.03	45.30	44.76	1.01
S-Wd-Wr-UE	84	80	1.05	10.22	8.85	1.15	230.57	228.90	1.01	43.82	42.92	1.02
Mean			1.05			1.31			1.03			1.02
SD			0.01			0.25			0.02			0.01
COV (%)			1.30			19.90			2.02			1.08

Table 7 bolsters the model's validity by comparing numerical results with experimental data. This comparison focuses on critical parameters such as P_{cr}, P_u, and their Δ_{cr} and Δ_u, respectively. The average ratio of (FE/EXP.) at cracking and ultimate load of 1.04. and 1.03 was observed. Furthermore, Fig. 10 shows good accuracy of the prediction between the FE modeling and experimental data in the form of crack patterns. The FEMs successfully capture the behavior observed in the experiments, including accurately simulating various failure modes and crack propagation patterns. This ability to replicate complex phenomena strengthens the credibility of the models as reliable tools for analysis. In conclusion, the validation process convincingly demonstrates the high accuracy and reliability of the FEMs. This success establishes their suitability for analyzing and predicting the structural behavior of similar specimens in future applications.

5 Parametric Study

A parametric study has been conducted to investigate the effect of strengthening thickness on the RC slab under punching force employing different HPCs and mesh reinforcement. The study has been applied to the three validated models: S-Wd-UE, S-Wd-US, and S-Wd-Wr-UE, which were strengthened with the mentioned UHP-ECC reinforced with Wd, UHP-SFRC reinforced with Wd and UHP-ECC reinforced with Wr, respectively. The chart shown in Fig. 11 illustrates the relationship between the ratio of strengthening layer thickness to slab depth (i.e., t_s/d) and the ultimate punching shear load capacity for three distinct validated models.

Generally, the ultimate punching capacity increased for all models as the ts/d ratio of strengthening increased, indicating the significant influence of strengthening thickness on the structural performance. However, both techniques use UHP-SFRC reinforced with Wd and UHP-ECC reinforced with Wd and Wr, which exhibit superior performance with similar ultimate capacities for most ratios. An optimal ratio is identified at 0.22, 0.28, and 0.32 for the three regimes used: UHP-ECC reinforced with Wd, UHP-SFRC reinforced with Wd, and UHP-ECC reinforced with Wd combined with Wr, respectively. Beyond this threshold, the increase in ultimate capacity plateaus for all models may be attributed to the transformation of flexural failure. Therefore, the use of UHP-ECC reinforced with Wd and Wr strengthening layer with a thickness ratio of 0.22 achieved near-maximal punching shear capacity without excessive material usage. Beyond this ratio, there is a limited increase in ultimate capacity. Thus, cost and material efficiency should prioritize this threshold for practical applications. This analysis helps engineers make informed decisions on the effective use of strengthening layers to enhance punching shear resistance while maintaining efficiency in material usage.

6 Conclusions

This paper presents a study on the use of UHP-ECC and UHP-SFRC as a bonded layer to the compression side of the slab as indirect flexural strengthening and bonded threaded steel rods as direct shear strengthening through slab thickness to augment the punching shear strength of the interior slab–column connection. The following conclusions are made based on the data generated from this research program.

- The unstrengthened slab–column connection and those with combined UHP-ECC or UHP-SFRC layer and steel bolts experienced pure punching shear failure with radial crack pattern and signs of concrete peeling or popping out along a significant portion of the perimeter of the cone-shaped perforation, showing circumferential cracks. On the other hand, the

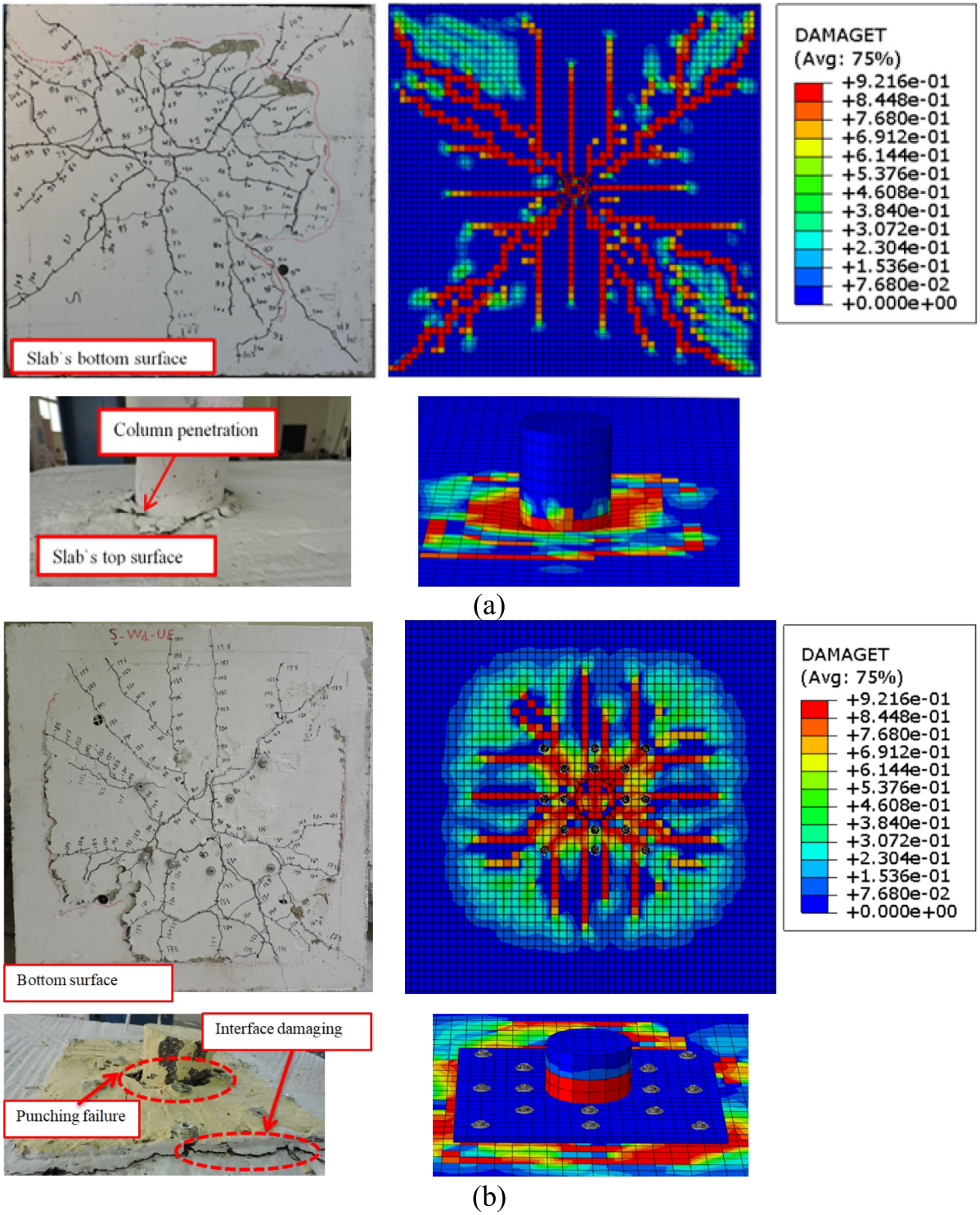

Fig. 10 FE versus experimental crack pattern and failure mode for selected slabs: **a** S slab; and f **b** S-Wd-UE slab

UHP-ECC strengthened slab with two layers of steel mesh experienced a combined flexure and punching shear failure since the increase in flexural capacity locally around the column delayed the sudden punching shear failure to a greater applied load.

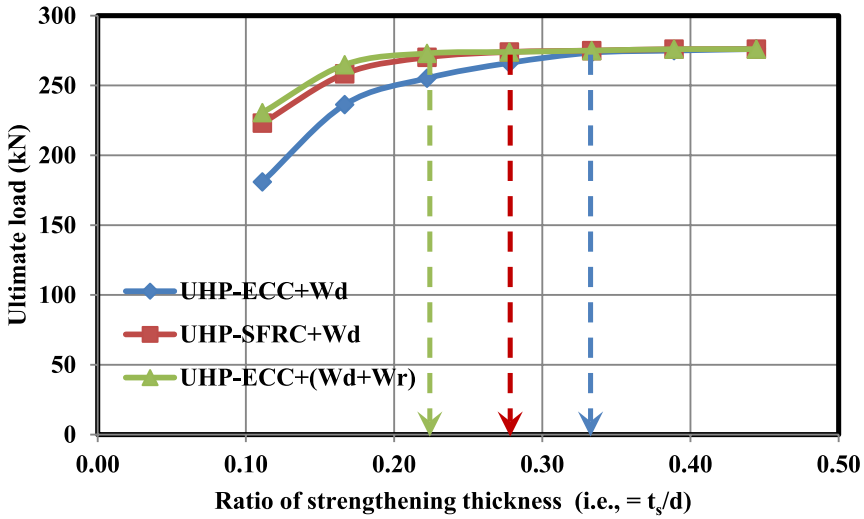

Fig. 11 Parametric study on P_u and strengthening layer with t_s/d ratio

- No debonding failure in the UHPC layer at its connection with the compression side of the slab was observed for all the tested slabs. In addition, no failure in the bonded steel bolts was observed. Moreover, the UHPC layer did not experience crushing before punching shear failure. These findings demonstrate the effectiveness of the proposed strengthening technique.
- The cracking and ultimate loads increased by an average of 16.5% and 47% when strengthening the slab with GWWM-reinforced UHP-ECC and UHP-SFRC, respectively. These values significantly increased when using WSM mesh due to changes in mesh mechanical properties.
- Strengthening the slab with GWWM-reinforced UHP-ECC and UHP-SFRC layer increased the elastic stiffness by 101% and 83% compared to the unstrengthened slab. A similar trend was noted for the energy consumed to reach the ultimate load, as it increased between 109 and 161% using the GWWM-reinforced UHP-ECC and UHP-SFRC layers, respectively. A similar conclusion was reached using WSM or double mesh in the UHPC layer.
- UHP-SFRC demonstrated superior performance compared to UHP-ECC in this testing, attributed to differences in their mechanical properties. Comparisons with experimental data showed that FEM predictions closely matched the test results, with the average ratio of predicted to actual load being nearly equal to one.
- Using UHP-ECC reinforced with Wd and Wr at a 0.22 thickness ratio optimizes punching shear capacity, achieving near-maximal strength efficiently. Beyond this, thickness increases yield negligible capacity gains, making 0.22 the optimal cost-effective threshold for punching strengthening.

Acknowledgements
Thanks to the technicians of the Concrete Structures Laboratory at Kafrelsheikh University in Egypt for their help.

Author contributions
Ahmed Hamoda: conceptualization, methodology, software, validation, formal analysis, investigation, data curation, writing—original draft, visualization, project administration. Khaled Sennah: writing—original draft, visualization, data curation. Mizan Ahmed: writing—review and editing, visualization. Aref A. Abadel: visualization, writing—review and editing. Mohamed Emara: software, investigation, data curation, formal analysis, writing—original draft.

Funding
The research has been completed with support under the Researchers Supporting Project number (RSP2025R343) supported by King Saud University, Riyadh, Saudi Arabia.

Availability of data and materials
The datasets used and/or analyzed during the current study are available from the corresponding author upon reasonable request.

Declarations

Ethics approval and consent to participate
Not applicable.

Consent for publication
Not applicable.

Competing interests
The authors declare that they have no competing interests.

Author details
[1]Civil Engineering Department, Faculty of Engineering, Kafrelsheikh University, Kafrelsheikh, Egypt. [2]Department of Civil Engineering, Toronto Metropolitan University, Toronto, ON, Canada. [3]Centre for Infrastructure Monitoring and Protection, School of Civil and Mechanical Engineering, Curtin University, Kent

Street, Bentley, WA 6102, Australia. [4]Department of Civil Engineering, College of Engineering, King Saud University, 11421 Riyadh, Saudi Arabia. [5]Structural Engineering Department, Faculty of Engineering, Zagazig University, B.O. Box 44519, Zagazig, Sharkia, Egypt. [6]Department of Civil Engineering, Delta Higher Institute for Engineering & Technology, Talkha, Egypt.

Received: 31 July 2024 Accepted: 3 February 2025
Published online: 21 July 2025

References

Abdel-Kareem, H. (2020). Punching strengthening of concrete slab-column connections using near surface mounted (NSM) carbon fiber reinforced polymer (CFRP) bars. *Journal of Engineering Research and Reports, 9*(2), 1–14. https://doi.org/10.9734/jerr/2019/v9i217013

Abdullah, A., & Bailey, C. (2018). Punching behaviour of column-slab connection strengthened with non-prestressed or prestressed FRP plates. *Engineering Structures, 160*, 229–242. https://doi.org/10.1016/j.engstruct.2018.01.030

Abdullah, A., Bailey, C., & Wu, Z. (2013). Tests investigating the punching shear of a column-slab connection strengthened with non-prestressed or prestressed FRP plates. *Construction and Building Materials, 48*, 1134–1144. https://doi.org/10.1016/j.conbuildmat.2013.07.012

Abdulrahman, B. Q., & Aziz, O. Q. (2021). Strengthening RC flat slab-column connections with FRP composites: A review and comparative study. *Journal of King Saud University-Engineering Sciences, 33*(7), 471–481. https://doi.org/10.1016/j.jksues.2020.07.005

Abdulrahman, B. Q., Wu, Z., & Cunningham, L. S. (2017). Experimental and numerical investigation into strengthening flat slabs at corner columns with externally bonded CFRP. *Construction and Building Materials, 139*, 132–147. https://doi.org/10.1016/j.conbuildmat.2017.02.056

ACI 440.2R-17. Guide for the design and construction of externally bonded FRP systems for strengthening concrete structures. (2017). In. American Concrete Institute, Farmington Hills, MI, USA.

ACI 318–19-Building Code Requirements for Reinforced Concrete. (2019). In. American Concrete Institute, Farmington Hills, MI, USA.

Afefy, H. M., & El-Tony, E.-T.M. (2019). Retrofitting of interior slab-to-column connections for punching shear using different techniques. *Journal of Performance of Constructed Facilities, 33*(1), 04018088. https://doi.org/10.1061/(ASCE)CF.1943-5509.0001246

Akhundzada, H., Donchev, T., & Petkova, D. (2019). Strengthening of slab-column connection against punching shear failure with CFRP laminates. *Composite Structures, 208*, 656–664. https://doi.org/10.1016/j.compstruct.2018.09.076

Al-Mawed, L. K., & Hamad, B. S. (2023). Experimental and numerical assessments of slab-column connections strengthened using bonded hemp fiber fabric sheets. *International Journal of Concrete Structures and Materials, 17*(1), 8. https://doi.org/10.1186/s40069-022-00567-z

Amiri, S., & Talaeitaba, S. B. (2020). Punching shear strengthening of flat slabs with EBROG and EBRIG–FRP strips. *Structures, 26*, 139–155. https://doi.org/10.1016/j.istruc.2020.04.017

Azizi, R., & Talaeitaba, S. B. (2019). Punching shear strengthening of flat slabs with CFRP on grooves (EBROG) and external rebars sticking in grooves. *International Journal of Advanced Structural Engineering, 11*(1), 79–95. https://doi.org/10.1007/s40091-019-0218-4

Binici, B., & Bayrak, O. (2003). Punching shear strengthening of reinforced concrete flat plates using carbon fiber reinforced polymers. *Journal of Structural Engineering, 129*(9), 1173–1182. https://doi.org/10.1061/(ASCE)0733-9445(2003)129:9(1173)

Bolešová, M., & Gajdošová, K. (2023). Experimental evaluation of flat slabs strengthened with post-installed shear bolts with pre-loading. *Engineering Structures, 293*, 116659. https://doi.org/10.1016/j.engstruct.2023.116659

Carreira, D. J., & Chu, K.-H. (1985). Stress-strain relationship for plain concrete in compression. *ACI Structural Journal, 82*(6), 797–804.

Chen, B., Zhou, J., Zhang, D., Sennah, K., & Nuti, C. (2023). Shear performances of reinforced ultra-high performance concrete short beams. *Engineering Structures, 277*, 115407. https://doi.org/10.1016/j.engstruct.2022.115407

Chen, B., Zhou, J., Zhang, D., Su, J., Nuti, C., & Sennah, K. (2022). Experimental study on shear performances of ultra-high performance concrete deep beams. *Structures, 39*, 310–322. https://doi.org/10.1016/j.istruc.2022.03.019

Chen, C.-C., & Chen, S.-L. (2019). Strengthening of reinforced concrete slab-column connections with carbon fiber reinforced polymer laminates. *Applied Sciences, 10*(1), 265. https://doi.org/10.3390/app10010265

Chen, C.-C., & Li, C.-Y. (2005). Punching shear strength of reinforced concrete slabs strengthened with glass fiber-reinforced polymer laminates. *ACI Structural Journal, 102*(4), 535.

da Silva Rodrigues, H. L., da Silva, P. M., & de Oliveira, D. R. C. (2015). Flat slabs strengthened to punching with carbon fiber reinforced polymer (CFRP) dowels. *Acta Scientiarum. Technology, 37*(4), 323–330.

Dat, P. X., & Hieu, N. T. (2023). Experimental study on the effectiveness of strengthening reinforced concrete slab-column connections using CFRP sheets. *Journal of Science and Technology in Civil Engineering (JSTCE)-HUCE, 17*(3), 46–54. https://doi.org/10.31814/stce.huce2023-17(3)-04

Durucan, C., & Anil, Ö. (2015). Effect of opening size and location on the punching shear behavior of interior slab–column connections strengthened with CFRP strips. *Engineering Structures, 105*, 22–36. https://doi.org/10.1016/j.engstruct.2015.09.033

El-Enein, H. A., Azimi, H., Sennah, K., & Ghrib, F. (2014). Flexural strengthening of reinforced concrete slab–column connection using CFRP sheets. *Construction and Building Materials, 57*, 126–137. https://doi.org/10.1016/j.conbuildmat.2014.01.077

El-Kashif, K. F., Ahmed, E. A., & Salem, H. M. (2019). Experimental investigation of strengthening slab-column connections with CFRP fan. *Ain Shams Engineering Journal, 10*(3), 639–650. https://doi.org/10.1016/j.asej.2019.02.005

El-Salakawy, E., Soudki, K., & Polak, M. A. (2004). Punching shear behavior of flat slabs strengthened with fiber reinforced polymer laminates. *Journal of Composites for Construction, 8*(5), 384–392. https://doi.org/10.1061/(ASCE)1090-0268(2004)8:5(384)

El-Sayed, K., Khalil, N., & Omar, M. (2016). Repair and strengthening of RC flat slab connection with edge columns against punching shear. *Advances in Research, 8*(3), 1–22. https://doi.org/10.9734/AIR/2016/30352

Elsayed, M., Abdel-Hady, I., Abdel-Hafez, L., & Tawfic, Y. R. (2022). Strengthening of slab-column connections using ultra high-performance fiber concrete. *Case Studies in Construction Materials, 17*, e01710. https://doi.org/10.1016/j.cscm.2022.e01710

Eltaly, B. A., Shaheen, Y. B., Salem, M., & Hamoda, A. (2024). Ferrocement oil pipes exposed to critical conditions and using various types of reinforcement mesh: Experimental and numerical studies. *Structures, 66*, 106780.

Erdogan, H., Binici, B., & Ozcebe, G. (2010). Punching shear strengthening of flat-slabs with CFRP dowels. *Magazine of Concrete Research, 62*(7), 465–478. https://doi.org/10.1680/macr.2010.62.7.465

Farghaly, A. S., & Ueda, T. (2011). Prediction of punching shear strength of two-way slabs strengthened externally with FRP sheets. *Journal of Composites for Construction, 15*(2), 181–193. https://doi.org/10.1061/(ASCE)CC.1943-5614.0000177

Faria, D. M., Einpaul, J., Ramos, A. M., Ruiz, M. F., & Muttoni, A. (2014). On the efficiency of flat slabs strengthening against punching using externally bonded fibre reinforced polymers. *Construction and Building Materials, 73*, 366–377. https://doi.org/10.1016/j.conbuildmat.2014.09.084

Fernández Ruiz, M., Muttoni, A., & Kunz, J. (2010). Strengthening of flat slabs against punching shear using post-installed shear reinforcement. *ACI Structural Journal, 107*(4), 434–442.

Halabi, Z., Ghrib, F., El-Ragaby, A., & Sennah, K. (2013). Behavior of RC slab-column connections strengthened with external CFRP sheets and subjected to eccentric loading. *Journal of Composites for Construction, 17*(4), 488–496. https://doi.org/10.1061/(ASCE)CC.1943-5614.0000343

Hamoda, A., Shahin, R. I., Ahmed, M., Abadel, A. A., & Yehia, S. A. (2024e). Flexural behavior of normal concrete circular beams strengthened using engineered cementitious composite and stainless steel tube. *Magazine of Concrete Research, in press*.

Hamoda, A., Abadel, A. A., Ahmed, M., Wang, V., Vrcelj, Z., & Liang, Q. Q. (2025). Punching shear performance of reinforced concrete slab-to-steel column connections incorporating ECC and UHPECC. *Engineering Structures, 322*, 119145.

Hamoda, A., Abadel, A. A., Sennah, K., Ahmed, M., Zhang, X., & Emara, M. (2024a). Shear strengthening of rc beams incorporating post-tensioned bars and engineered cementitious composite reinforced with palm fronds. *Buildings, 14*(10), 3277.

Hamoda, A. A., Ahmed, M., Abadel, A. A., Ghalla, M., Patel, V. I., & Liang, Q. Q. (2023c). Experimental and numerical studies of circular precast concrete slender columns with intermediate connection filled with high-performance concrete. *Structures, 57*, 105204.

Hamoda, A., Ahmed, M., Abadel, A. A., & Gohari, S. (2024b). Experimental and numerical investigations of precast circular reinforced concrete slender columns with intermediate connection. *Advances in Structural Engineering, 27*(3), 373–385.

Hamoda, A., Ahmed, M., Ghalla, M., Liang, Q. Q., & Abadel, A. A. (2023a). Flexural performance of precast circular reinforced concrete members with intermediate connection filled with ultra-high-performance-concrete. *Case Studies in Construction Materials, 19*, e02386.

Hamoda, A., Ahmed, M., & Sennah, K. (2023b). Experimental and numerical investigations of the effectiveness of engineered cementitious composites and stainless steel plates in shear strengthening of reinforced concrete beams. *Structural Concrete, 24*(2), 2778–2799. https://doi.org/10.1002/suco.202200226

Hamoda, A., Fayed, S., Mansour, W., & Emara, M. (2024c). Behavior of reinforced concrete circular columns subjected to double curvature buckling moment. *International Journal of Concrete Structures and Materials, 18*(1), 70.

Hamoda, A., Sennah, K., Abadel, A. A., & Emara, M. (2024d). Strengthening of interior circular column-slab region incorporating combinations of bonded UHPECC layer, CFRP sheets, and threaded steel bolts. *Structures, 69*, 107545.

Hamoda, A., Yehia, S. A., Abadel, A. A., Sennah, K., & Shahin, R. I. (2024). Strengthening of simply supported deep beams with openings using steel-reinforced ECC and externally bonded CFRP sheets. *Magazine of Concrete Research, 1*, 1–17.

Harajli, M., & Soudki, K. (2003). Shear strengthening of interior slab–column connections using carbon fiber-reinforced polymer sheets. *Journal of Composites for Construction, 7*(2), 145–153. https://doi.org/10.1061/(ASCE)1090-0268(2003)7:2(145)

Harajli, M., Soudki, K., & Kudsi, T. (2006). Strengthening of interior slab–column connections using a combination of FRP sheets and steel bolts. *Journal of Composites for Construction, 10*(5), 399–409. https://doi.org/10.1061/(ASCE)1090-0268(2006)10:5(399)

Hou, L., Xu, R., Chen, D., Xu, S., & Aslani, F. (2020). Seismic behavior of reinforced engineered cementitious composite members and reinforced concrete/engineered cementitious composite members: A review. *Structural Concrete, 21*(1), 199–219. https://doi.org/10.1002/suco.201800269

Jafarian, N., Mostofinejad, D., & Naderi, A. (2020). Effects of FRP grids on punching shear behavior of reinforced concrete slabs. *Structures, 28*, 2523–2536. https://doi.org/10.1016/j.istruc.2020.10.061

Jang, J.-I., & Kang, S.-M. (2019). Punching shear behavior of shear reinforced slab–column connection with varying flexural reinforcement. *International Journal of Concrete Structures and Materials, 13*, 1–14. https://doi.org/10.1186/s40069-019-0341-4

Joh, C., Hwang, H., & Kim, B. (2008). Punching shear and flexural strengths of ultra high performance concrete slabs. *High Performance Structures and Materials IV, 97*, 97–106. https://doi.org/10.2495/HPSM080111

Kadhim, M. M., Saleh, A. R., Cunningham, L. S., & Semendary, A. A. (2021). Numerical investigation of non-shear-reinforced UHPC hybrid flat slabs subject to punching shear. *Engineering Structures, 241*, 112444. https://doi.org/10.1016/j.engstruct.2021.112444

Kim, H., Moon, B., Hu, X., Lee, H., Ryu, G.-S., Koh, K.-T., . . . Keierleber, B. (2021). Construction and performance monitoring of innovative ultra-high-performance concrete bridge. *Infrastructures, 6*(9), 121. https://doi.org/10.3390/INFRASTRUCTURES6090121.

Koppitz, R., Kenel, A., & Keller, T. (2014). Punching shear strengthening of flat slabs using prestressed carbon fiber-reinforced polymer straps. *Engineering Structures, 76*, 283–294. https://doi.org/10.1016/j.engstruct.2014.07.017

Lampropoulos, A., Tsioulou, O., Mina, A., Nicolaides, D., & Petrou, M. F. (2023). Punching shear and flexural performance of ultra-high performance fibre reinforced concrete (UHPFRC) slabs. *Engineering Structures, 281*, 115808. https://doi.org/10.1016/j.engstruct.2023.115808

Lapi, M., Fernandes, H., Orlando, M., Ramos, A., & Lúcio, V. (2018). Performance assessment of flat slabs strengthened with a bonded reinforced-concrete overlay. *Magazine of Concrete Research, 70*(9), 433–451. https://doi.org/10.1680/jmacr.17.00037

Lapi, M., Ramos, A. P., & Orlando, M. (2019). Flat slab strengthening techniques against punching-shear. *Engineering Structures, 180*, 160–180. https://doi.org/10.1016/j.engstruct.2018.11.033

Lawler, N., & Polak, M. A. (2011). Development of FRP shear bolts for punching shear retrofit of reinforced concrete slabs. *Journal of Composites for Construction, 15*(4), 591–601. https://doi.org/10.1061/(ASCE)CC.1943-5614.0000188

Li, C., Chen, B., Sennah, K., Liu, J., & Liao, M. (2023). Experimental study on axial compressive behavior of stone masonry with ultra-high performance mortar. *Materials and Structures, 56*(7), 124. https://doi.org/10.1617/s11527-023-02215-8

Li, R., Cho, Y. S., & Zhang, S. (2007). Punching shear behavior of concrete flat plate slab reinforced with carbon fiber reinforced polymer rods. *Composites Part b: Engineering, 38*(5–6), 712–719. https://doi.org/10.1016/j.compositesb.2006.07.017

Meisami, M. H., Mostofinejad, D., & Nakamura, H. (2013). Punching shear strengthening of two-way flat slabs using CFRP rods. *Composite Structures, 99*, 112–122. https://doi.org/10.1016/j.compstruct.2012.11.028

Meisami, M. H., Mostofinejad, D., & Nakamura, H. (2014). Punching shear strengthening of two-way flat slabs with CFRP grids. *Journal of Composites for Construction, 18*(2), 04013047. https://doi.org/10.1061/(ASCE)CC.1943-5614.0000443

Meisami, M. H., Mostofinejad, D., & Nakamura, H. (2015). Strengthening of flat slabs with FRP fan for punching shear. *Composite Structures, 119*, 305–314. https://doi.org/10.1016/j.compstruct.2014.08.041

Muttoni, A. (2008). Punching shear strength of reinforced concrete slabs without transverse reinforcement. *ACI Structural Journal, 105*(4), 440–450.

Polies, W., Ghrib, F., & Sennah, K. (2010). Rehabilitation of interior reinforced concrete slab–column connections using CFRP sheets. *Construction and Building Materials, 24*(7), 1272–1285. https://doi.org/10.1016/j.conbuildmat.2009.12.008

Qian, K., & Li, B. (2013). Strengthening and retrofitting of RC flat slabs to mitigate progressive collapse by externally bonded CFRP laminates. *Journal of Composites for Construction, 17*(4), 554–565. https://doi.org/10.1061/(ASCE)CC.1943-5614.0000352

Said, M., Adam, M. A., Arafa, A. E., & Moatasem, A. (2020). Improvement of punching shear strength of reinforced lightweight concrete flat slab using different strengthening techniques. *Journal of Building Engineering, 32*, 101749.

Saleh, H., Abdouka, K., Al-Mahaidi, R., & Kalfat, R. (2018a). Strengthening of slab–column connections against punching shear using FRP materials: State-of-the-art review. *Australian Journal of Structural Engineering, 19*(3), 188–206. https://doi.org/10.1080/13287982.2018.1462901

Saleh, H., Kalfat, R., Abdouka, K., & Al-Mahaidi, R. (2018b). Experimental and numerical study into the punching shear strengthening of RC flat slabs using post-installed steel bolts. *Construction and Building Materials, 188*, 28–39. https://doi.org/10.1016/j.conbuildmat.2018.08.064

Santos, G. S., Melo, G. S., & Barros, J. A. (2019). Punching CFRP-based strengthening solutions for reinforced concrete flat slabs. *Composite Structures, 224*, 111077. https://doi.org/10.1016/j.compstruct.2019.111077

Silva, M., Dedigamuwa, K., & Gamage, J. (2021). Performance of severely damaged reinforced concrete flat slab-column connections strengthened with Carbon Fiber Reinforced Polymer. *Composite Structures, 255*, 112963. https://doi.org/10.1016/j.compstruct.2020.112963

Silva, M., Gamage, J., & Fawzia, S. (2019). Performance of slab-column connections of flat slabs strengthened with carbon fiber reinforced polymers. *Case Studies in Construction Materials, 11*, e00275. https://doi.org/10.1016/j.cscm.2019.e00275

Sissakis, K., & Sheikh, S. A. (2007). Strengthening concrete slabs for punching shear with carbon fiber-reinforced polymer laminates. *ACI Structural Journal, 104*(1), 49.

Smith, S. T., Hu, S., Kim, S. J., & Seracino, R. (2011). FRP-strengthened RC slabs anchored with FRP anchors. *Engineering Structures, 33*(4), 1075–1087. https://doi.org/10.1016/j.engstruct.2010.11.018

Song, J.-K., Kim, J., Song, H.-B., & Song, J.-W. (2012). Effective punching shear and moment capacity of flat plate-column connection with shear reinforcements for lateral loading. *International Journal of Concrete Structures and Materials, 6*, 19–29. https://doi.org/10.1007/s40069-012-0002-3

Su, J.-Z., Ma, X.-L., Chen, B.-C., & Sennah, K. (2020). Full-scale bending test and parametric study on a 30-m span prestressed ultra-high performance

concrete box girder. *Advances in Structural Engineering, 23*(7), 1276–1289. https://doi.org/10.1177/1369433219894244

Taresh, H., Yatim, M., & Azmi, M. (2021). Punching shear behaviour of interior slab-column connections strengthened by steel angle plates. *Engineering Structures, 238*, 112246. https://doi.org/10.1016/j.engstruct.2021.112246

Torabian, A., Isufi, B., Mostofinejad, D., & Pinho Ramos, A. (2021). Shear and flexural strengthening of deficient flat slabs with post-installed bolts and CFRP composites bonded through EBR and EBROG. *Structural Concrete, 22*(2), 1147–1164.

Torabian, A., Isufi, B., Mostofinejad, D., & Ramos, A. P. (2020). Flexural strengthening of flat slabs with FRP composites using EBR and EBROG methods. *Engineering Structures, 211*, 110483. https://doi.org/10.1016/j.engstruct.2020.110483

Yagar, A. C., Derogar, S., Ince, C., & Ball, R. J. (2024). Evaluation of ACI code equation on punching shear strength of slab-column connections strengthened with FRP: A database study. *Engineering Structures, 308*, 117965. https://doi.org/10.1016/j.engstruct.2024.117965

Yehia, E., Khalil, A. H., Mostafa, E.-E., & El-Nazzer, M. A. (2023). Experimental and numerical investigation on punching behavior of ultra-high performance concrete flat slabs. *Ain Shams Engineering Journal, 14*(10), 102208. https://doi.org/10.1016/J.ASEJ.2023.102208

Zhang, H., & Smith, S. T. (2012). FRP-to-concrete joint assemblages anchored with multiple FRP anchors. *Composite Structures, 94*(2), 403–414. https://doi.org/10.1016/j.compstruct.2011.07.025

Zhou, J., Pan, J., & Leung, C. K. (2015). Mechanical behavior of fiber-reinforced engineered cementitious composites in uniaxial compression. *Journal of Materials in Civil Engineering, 27*(1), 04014111.

Zhou, S., Xie, L., Jia, Y., & Wang, C. (2020). Review of cementitious composites containing polyethylene fibers as repairing materials. *Polymers, 12*(11), 2624. https://doi.org/10.3390/polym12112624

Zohrevand, P., Yang, X., Jiao, X., & Mirmiran, A. (2015). Punching shear enhancement of flat slabs with partial use of ultrahigh-performance concrete. *Journal of Materials in Civil Engineering, 27*(9), 04014255. https://doi.org/10.1061/(ASCE)MT.1943-5533.0001219

Publisher's Note

Ahmed Hamoda Assistant Professor, Civil Engineering Department, Faculty of Engineering, Kafrelsheikh University, Kafrelsheikh, Egypt.

Khaled Sennah Professor, Department of Civil Engineering, Toronto Metropolitan University, Toronto, Ontario, Canada.

Mizan Ahmed Senior Lecturer, Centre for Infrastructure Monitoring and Protection, School of Civil and Mechanical Engineering, Curtin University, Kent Street, Bentley, WA 6102, Australia.

Aref A. Abadel Associate Professor, Department of Civil Engineering, College of Engineering, King Saud University, Riyadh 11421, Saudi Arabia.

Mohamed Emara Associate Professor, Structural Engineering Department, Faculty of Engineering, Zagazig University, B.O. Box 44519, Zagazig, Sharkia, Egypt; Department of Civil Engineering, Delta Higher Institute for Engineering & Technology, Talkha, Egypt.